Exponential Chaotic Model for Generating Robust Chaos

Zhongyun Hua, *Member, IEEE*, and Yicong Zhou, *Senior Member, IEEE*

***Abstract*—Robust chaos is defined as the inexistence of periodic windows and coexisting attractors in the neighborhood of parameter space. This characteristic is desired because a chaotic system with robust chaos can overcome the chaos disappearance caused by parameter disturbance in practical applications. However, many existing chaotic systems fail to consider the robust chaos. This article introduces an exponential chaotic model (ECM) to produce new one-dimensional (1-D) chaotic maps with robust chaos. ECM is a universal framework and can produce many new chaotic maps employing any two 1-D chaotic maps as base and exponent maps. As examples, we present nine chaotic maps produced by ECM, discuss their bifurcation diagrams and prove their robust chaos. Performance evaluations also show that these nine chaotic maps of ECM can obtain robust chaos in a large parameter space. To show the practical applications of ECM, we employ these nine chaotic maps of ECM in secure communication. Simulation results show their superior performance against various channel noise during data transmission.**

***Index Terms*—Chaotic behavior, chaotic system, nonlinear system, robust chaos, secure communication.**

I. Introduction

CHAOS theory focuses on the chaotic behaviors that are sensitive to the changes in initial states [1]. The chaotic behavior was first noticed by Lorenz [2] in meteorology. Subsequently, researchers have observed chaotic behaviors in different types of natural and nonnatural phenomena, such as the cluster of stars and the change of electricity [3], [4]. According to the definition in [5], a dynamical system shows chaotic behaviors if it has the properties as follows: 1) sensitivity to its initial states; 2) topological transitivity; and 3) density of periodic orbits. With these unique properties, chaotic systems are widely studied and applied to many applications [6]–[9], especially in data security [10]–[12] and nonlinear control [13], [14]. This is because chaotic systems have general characteristics with these applications [15]–[17].

When studying chaos theory and applying chaotic systems to real applications, researchers have found that existing chaotic systems may have disadvantages in several aspects [18]. First, chaos degradation may occur when chaotic systems are digitized, because the precision of all the software and hardware platforms is finite [19]. Theoretically, the approaching states of a chaotic system locally oscillate in its phase plane. However, they may overlap when being digitized in real platforms. Then the chaotic behaviors may degrade to regular behaviors [20]. The chaos degradation brings seriously negative influences to the chaos-based applications [21]. Second, with the quick increment of computer ability and fast development of chaos theory, many chaotic behaviors with low degree of complexity can be estimated [22], [23]. The commonly used strategies of estimating chaotic behaviors are to predict their chaotic signals [24] and to identify their initial states [25]. In addition, existing chaotic systems may not have robust chaos [26]. The robust chaos is extremely important for many chaos-based applications, because a chaotic system owning robust chaos can avoid the chaos degradation caused by parameter perturbations [27], [28].

At present, many research works have focused on improving the chaos complexity of chaotic systems [29], [30]. These efforts can be classified into two types: 1) perturbing the chaotic signals of chaotic systems and 2) designing new chaotic systems. The first type of efforts can significantly delay the chaos degradation. Deng *et al.* [31] proposed a feedback control method to enhance the complexity of chaotic signals. Li *et al.* [32] presented a reseeding mixing technology to enlarge the periods of chaotic signals. The reseeding concept is to remove the chaotic signals with short periods from the system while the mixing concept is to enlarge the periods of chaotic signals. The second type of efforts can obtain new chaotic systems with higher complexity [33], [34]. Huang *et al.* [35] introduced a grid multiwing butterfly chaotic attractor, which is generated by replacing the state variables in the Lorenz system using piecewise hysteresis functions. In [36], a unified approach was proposed to design hyperchaotic systems with desired property. Shen and Jia [37] first investigated the conditions of generating one-dimensional (1-D) discrete chaotic systems, and

Manuscript received December 31, 2018; revised April 30, 2019; accepted July 17, 2019. Date of publication August 28, 2019; date of current version May 18, 2021. This work was supported in part by the National Key Research and Development Program of China under Grant 2018YFB1003800 and Grant 2018YFB1003805, in part by the National Natural Science Foundation of China under Grant 61701137, in part by the Shenzhen Science and Technology Program under Grant JCYJ20170307150704051 and Grant JCYJ20170811160212033, in part by the Science and Technology Development Fund, Macau SAR, under Grant 189/2017/A3, and in part by the Research Committee at University of Macau under Grant MYRG2016-00123-FST and Grant MYRG2018-00136-FST. This article was recommended by Associate Editor C. K. Ahn. *(Corresponding authors: Yicong Zhou; Zhongyun Hua.)*

Z. Hua is with the School of Computer Science and Technology, Harbin Institute of Technology Shenzhen, Shenzhen 518055, China (e-mail: huazyum@gmail.com; huazhongyun@hit.edu.cn).

Y. Zhou is with the Department of Computer and Information Science, University of Macau, Macau 999078, China (e-mail: yicongzhou@um.edu.mo).

Color versions of one or more figures in this article are available at https://doi.org/10.1109/TSMC.2019.2932616.

Digital Object Identifier 10.1109/TSMC.2019.2932616

then constructed several new 1-D chaotic systems according to these conditions. This article significantly contributes to the development of discrete chaos. Although these efforts can reduce the negative effects of chaotic systems in practical applications, they still have some limitations. When using different technologies to perturb chaotic signals, the mathematical equations and integrality of chaotic systems may be broken. This leads the chaotic systems to lose some natural properties. For previous works of designing new chaotic systems, they fail to consider the robust chaos and thus the constructed chaotic systems cannot generate robust chaotic behaviors [33], [37]–[39]. The robust chaos is a desired property for many real applications. As a result, designing chaotic systems with robust chaos is a meaningful and attractive research topic.

To obtain 1-D chaotic maps with robust chaos, this article introduces an exponential chaotic model (ECM). Motivated by the concept of exponential operation in arithmetic, ECM can produce many new chaotic maps using 1-D chaotic maps as base and exponent maps. Theoretical analysis, experimental results, and real application are provided to prove the robust chaos and complex chaotic behaviors of the new chaotic maps generated by ECM. The contributions and novelty of this article are summarized as follows.

1) We propose ECM as a universal framework. Employing two 1-D chaotic maps as base and exponent maps, ECM can produce many new 1-D chaotic maps with robust chaos.
2) As examples, we present nine new chaotic maps generated by ECM. Theoretical analysis demonstrates their robust chaos.
3) We quantitatively evaluate the chaotic maps of ECM using Lyapunov exponent (LE), correlation dimension (CD), and initial state sensitivity. Experiment results show that these chaotic maps are sensitive to their initial states, and have robust chaotic behaviors in a large parameter space.
4) To show the practical application of ECM, we apply the nine chaotic maps of ECM to secure communication. Simulation results indicate that these maps exhibit better performance in resisting various channel noise than their base and exponent maps.

The rest of this article is organized as follows. Section II introduces three 1-D chaotic maps and the definition of robust chaos. Section III presents the proposed ECM and analyzes its dynamic properties. Section IV generates nine 1-D chaotic maps of ECM as examples, analyzes their bifurcation diagrams and proves their robust chaos. Section V evaluates the chaos complexity and performance of these chaotic maps of ECM and Section VI investigates their application in secure communication. Section VII concludes this article.

II. Preliminaries

This section reviews the logistic, tent and sine maps that are used as the base and exponent maps in the proposed ECM in Section IV. The definition of robust chaos is also presented as preliminary knowledge.

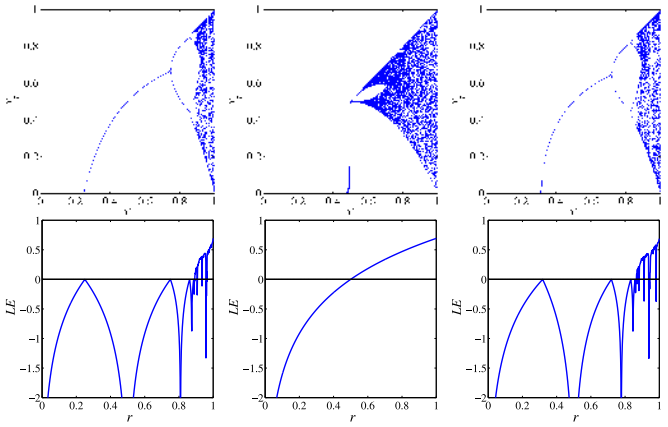

Fig. 1. Top row plots the bifurcation diagrams of the (a) logistic map, (b) tent map, and (c) sine map, and the bottom row plots their LEs.

A. Existing 1-D Chaotic Maps

The logistic map is designed to describe the change of population. By inputting a value within interval [0, 1], the output of the logistic map can oscillate in this range. The mathematical definition of the logistic map is described as

$$x_{i+1} = L(r, x_i) = 4rx_i(1 - x_i). \tag{1}$$

The variable r is a control parameter and it is on the interval [0, 1].

The tent map obtains an output on the interval [0, 1]. It stretches an input if the input is smaller than 0.5; otherwise, it folds it. The mathematical equation of the tent map is written as

$$x_{i+1} = T(r, x_i) = 2r \min\{x_i, 1 - x_i\}. \tag{2}$$

The variable r is a control parameter and it is also on the interval [0, 1].

The sine map is developed from the sine transform. By scaling an input with π, the sine map transforms an input on the interval [0, 1] into the same interval. It has the definition as

$$x_{i+1} = S(r, x_i) = r \sin(\pi x_i) \tag{3}$$

where variable r is a control parameter and it is also on the interval $r \in [0, 1]$.

Bifurcation diagram shows the occupied or approaching states by a dynamical system with the increment of its control parameter(s). The top row of Fig. 1 shows the bifurcation diagrams of the logistic, tent, and sine maps. The LE is an indicator of chaos [40] and the bottom row of Fig. 1 shows the LEs of the three chaotic maps. As can be seen, the logistic, tent, and sine maps show chaos properties in the parameter ranges [0.8925, 1], (0.5.1), and [0.8656, 1], respectively. The logistic and sine maps have similar bifurcation diagrams, because the Taylor series of $\sin(x)$ is a combination of polynomials. However, the logistic and sine maps are totally different chaotic maps with different definitions and behaviors.

B. Definition of Robust Chaos

The robust chaos is defined as the inexistence of periodic windows and coexisting attractors in the whole chaotic range [26]. The existence of the periodic windows in chaotic range indicates that a small change to the parameter will destroy the chaos, implying frail chaos. A chaotic system owning robust chaos can avoid the chaos degradation caused by the electromagnetic interference, noise pollution and other perturbations to the system parameters. Thus, the robust chaos is a desired property for chaos-based applications [41]. For example, when a chaotic system is used to describe a physical system, the robust chaos is required to correctly reflect whether the physical system has chaotic behaviors, because the digitized parameter is only an approximation of the real parameter value [42]. According to [26], a dynamical system can generate robust chaos if it does not have stable periodic orbits and has a unique chaotic attractor in the whole parameter space. The robust chaos of a dynamical system can be verified using strict mathematical theorem if it is differentiable.

First, we give the definition of 1-D discrete *S*-unimodal map, which is described as Definition 1 [26, Definition 11.7].

Definition 1: A map $f : I = [m, n] \to I$ is *S*-unimodal on I if it satisfies: 1) the function $f(x)$ is of class C^3; 2) $f(m) = f(n) = m$; 3) $f(x)$ has a unique local maximum at (m, n); and 4) $f(x)$ has a negative Schwarzian derivative for all $x \in I - \{y, f'(y) = 0\}$.

Then the occurrence of robust chaos for a 1-D discrete *S*-unimodal map can be described in Theorem 1 [26, Th. 11.12].

Theorem 1: Let $\varphi_\nu(x) : I = [m, n] \to I$ be a parametric 1-D discrete *S*-unimodal map with the unique maximum at $k \in (m, n)$ and $\varphi_\nu(k) = n \ \forall \nu \in (\nu_{\min}, \nu_{\max})$. Then $\varphi_\nu(x)$ generates robust chaos for $\nu \in (\nu_{\min}, \nu_{\max})$.

According to the property of the *S*-unimodal map [26, Th. 11.1], the parametric *S*-unimodal map $\varphi_\nu(x)$ for all $\nu \in (\nu_{\min}, \nu_{\max})$ follows that there is at most one attracting periodic orbit with the critical point in its basin of the attraction. In this case, the orbit with initial value $x_0 = k$ maps in two iterates to the fixed point $x = m$, because $\varphi_\nu(k) = n$ and $\varphi_\nu(n) = m$. The fixed point $x = m$ is unstable because

$$|\varphi'_\nu(m)| \geq \frac{\varphi_\nu(k) - \varphi_\nu(m)}{k - m} = \frac{n - m}{k - m} > 1.$$

Thus, the map $\varphi_\nu(x)$ does not have any stable periodic orbits and there is a unique chaotic attractor. This indicates that $\varphi_\nu(x)$ can generate robust chaos for all $\nu \in (\nu_{\min}, \nu_{\max})$. One can also see detailed analysis and proof of Theorem 1 in [26, Ch. 11.2.1].

One can easily prove that the logistic map in (1) and sine map in (3) are *S*-unimodal maps on the interval $[0, 1]$ and their unique maximum values can be obtained at $x = 0.5$. However, there does not exist a parameter interval $(\nu_{\min}, \nu_{\max})$ that satisfies $L(\nu, 0.5) = S(\nu, 0.5) = 1 \ \forall \nu \in (\nu_{\min}, \nu_{\max})$. Then, the logistic and sine maps cannot satisfy the requirements of Theorem 1 and they cannot generate robust chaos. As the tent map in (2) is an unsmooth map and has a corner at $x = 0.5$, Theorem 1 is not feasible to judge whether it has robust chaos.

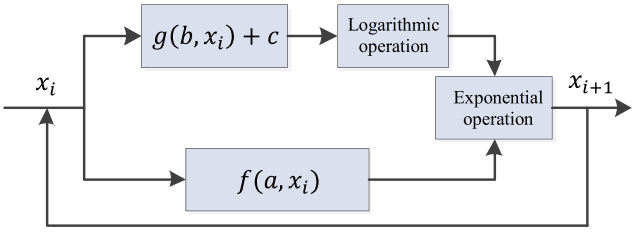

Fig. 2. Structure of ECM.

III. Exponential Chaotic Model

This section presents the proposed ECM and discusses its dynamic behaviors.

A. ECM

Motivated by the concept of exponential operation in arithmetic, we propose ECM to produce new 1-D chaotic maps using two 1-D chaotic maps as base and exponent maps. Fig. 2 presents the structure of ECM. As can be seen, the two maps $f(a, x_i)$ and $g(b, x_i)$ are the base and exponent maps, respectively, a and b are their control parameters, and c is a small bias to balance the output of $g(b, x_i)$.

The mathematical representation of ECM is written as

$$x_{i+1} = \mathcal{E}(x_i) = f(a, x_i)^{\ln(g(b,x_i)+c)}. \tag{4}$$

The outputs of ECM are generated in an iteration form. The variable x_i is simultaneously fed into the inputs of the base map $f(a, x_i)$ and exponent map $g(b, x_i)$. The base part is the output of $f(a, x_i)$ while the exponent part is the logarithm with base e to the combination of the output of $g(b, x_i)$ and the bias c.

Using one 1-D chaotic map as the base map and another 1-D chaotic map as the exponent map, ECM in (4) can achieve the following properties.

1) Users have flexibility to produce a large number of 1-D chaotic maps employing different combinations of the base map $f(a, x_i)$ and exponent map $g(b, x_i)$.
2) The base map $f(a, x_i)$ and exponent map $g(b, x_i)$ can be the identical or different 1-D chaotic maps. Even only exchanging the settings of $f(a, x_i)$ and $g(b, x_i)$, ECM can produce totally different chaotic maps, e.g., the TEL and LET maps in Table I.
3) The chaotic maps of ECM have a larger cycle length and can be less affected by digitization than their base and exponent maps. Supposing that the cycle lengths of the digitized base map $f(x)$ and digitized exponent map $g(x)$ are p and q, respectively, the cycle length of the digitized ECM $\mathcal{E}(x) = f(x)^{\ln(g(x)+c)}$ is the lowest common multiple of p and q.

B. Fixed Point and Stability Analysis

The fixed point is important characteristic of a dynamical system and it can reflect the dynamic property of the system. Here, we calculate the fixed points of ECM and investigate their stability. The fixed points of the dynamical system $x_{i+1} = f(x_i)$ are the roots of the equation $x_{i+1} = x_i$. Thus, the fixed

TABLE I
CHAOTIC MAPS PRODUCED BY ECM IN (4) USING THE LOGISTIC, TENT, AND SINE MAPS AS THE BASE AND EXPONENT MAPS

$f(a,x_i)$	$g(b,x_i)$	Chaotic maps of ECM	Definitions
$L(a,x_i)$	$L(b,x_i)$	logistic-exponent-logistic (LEL) map	$x_{i+1} = L(a,x_i)^{\ln(L(b,x_i)+c)} = (4ax_i(1-x_i))^{\ln(4bx_i(1-x_i)+c)}$
	$S(b,x_i)$	logistic-exponent-sine (LES) map	$x_{i+1} = L(a,x_i)^{\ln(S(b,x_i)+c)} = (4ax_i(1-x_i))^{\ln(b\sin(\pi x_i)+c)}$
	$T(b,x_i)$	logistic-exponent-tent (LET) map	$x_{i+1} = L(a,x_i)^{\ln(T(b,x_i)+c)} = (4ax_i(1-x_i))^{\ln(2b\min\{x_i,1-x_i\}+c)}$
$S(a,x_i)$	$L(b,x_i)$	sine-exponent-logistic (SEL) map	$x_{i+1} = S(a,x_i)^{\ln(L(b,x_i)+c)} = (a\sin(\pi x_i))^{\ln(4bx_i(1-x_i)+c)}$
	$S(b,x_i)$	sine-exponent-sine (SES) map	$x_{i+1} = S(a,x_i)^{\ln(S(b,x_i)+c)} = (a\sin(\pi x_i))^{\ln(b\sin(\pi x_i)+c)}$
	$T(b,x_i)$	sine-exponent-tent (SET) map	$x_{i+1} = S(a,x_i)^{\ln(T(b,x_i)+c)} = (a\sin(\pi x_i))^{\ln(2b\min\{x_i,1-x_i\}+c)}$
$T(a,x_i)$	$L(b,x_i)$	tent-exponent-logistic (TEL) map	$x_{i+1} = T(a,x_i)^{\ln(L(b,x_i)+c)} = (2a\min\{x_i,1-x_i\})^{\ln(4bx_i(1-x_i)+c)}$
	$S(b,x_i)$	tent-exponent-sine (TES) map	$x_{i+1} = T(a,x_i)^{\ln(S(b,x_i)+c)} = (2a\min\{x_i,1-x_i\})^{\ln(b\sin(\pi x_i)+c)}$
	$T(b,x_i)$	tent-exponent-tent (TET) map	$x_{i+1} = T(a,x_i)^{\ln(T(b,x_i)+c)} = (2a\min\{x_i,1-x_i\})^{\ln(2b\min\{x_i,1-x_i\}+c)}$

points of ECM, denoted as $\tilde{x}$, are the roots of the following equation:

$$\tilde{x} = \mathcal{E}(\tilde{x}) = f(a,\tilde{x})^{\ln(g(b,\tilde{x})+c)}. \tag{5}$$

The stability of a fixed point depends on the derivative J of the dynamical system at that point. The fixed point is a critical point and it is superstable when $J = 0$; it is stable when $0 < |J| < 1$; it is neutral when $|J| = 1$; and it is unstable and the attractors closing to the point will escape from it when $|J| > 1$. The derivative of ECM in (4) can be calculated as follows:

$$\begin{aligned} J &= \frac{d_{f(a,x_i)^{\ln(g(b,x_i)+c)}}}{d_{x_i}} \\ &= f(a,x_i)^{\ln(g(b,x_i)+c)}(\ln(g(b,x_i)+c)\ln(f(a,x_i)))' \\ &= f(a,x_i)^{\ln(g(b,x_i)+c)}\left(\frac{f'(a,x_i)\ln(g(b,x_i)+c)}{f(a,x_i)} + \frac{g'(b,x_i)\ln(f(a,x_i))}{g(b,x_i)+c}\right). \end{aligned} \tag{6}$$

Setting the base map $f(a,x_i)$ and exponent map $g(b,x_i)$ in (5) and (6) as existing 1-D chaotic maps, one can calculate out the fixed points and their related derivatives of the chaotic maps generated by ECM, and then can further deduce the dynamic behaviors of these chaotic maps.

IV. GENERATION OF NEW CHAOTIC MAPS

Setting the base and exponent maps as different 1-D chaotic maps, ECM can produce many new chaotic maps. This section produces nine chaotic maps of ECM employing the three existing chaotic maps introduced in Section II-A, and analyzes their bifurcation diagrams and robust chaos.

Table I lists the nine produced chaotic maps using ECM. When the base map $f(a,x_i)$ and exponent map $g(b,x_i)$ are chosen as an identical chaotic map, the chaotic map performs exponential operation with itself to obtain a new chaotic map, including the tent-exponent-tent (TET) map, logistic-exponent-logistic (LEL) map, and sine-exponent-sine (SES) map. When the base and exponent maps are selected as two chaotic maps, swapping the base and exponent maps can result in two completely different chaotic maps. For example, the tent-exponent-logistic (TEL) and logistic-exponent-tent (LET) maps. In addition, when two chaotic maps with similar behaviors are used in ECM, exchanging the settings of the base and exponent maps, ECM can also produce new chaotic maps with totally different chaotic behaviors. For example, the logistic-exponent-sine (LES) and sine-exponent-logistic (SEL) maps. All the chaotic maps of ECM have three control parameters a, b, and c. The parameters a and b are from their corresponding base and exponent maps, and they are on the interval $[0, 1]$, while the parameter c is a small bias of the system and it is on the interval $[2, 2.8]$. This article investigates the behaviors of these new chaotic maps in the parameter (b, c) space by setting $a = 1$.

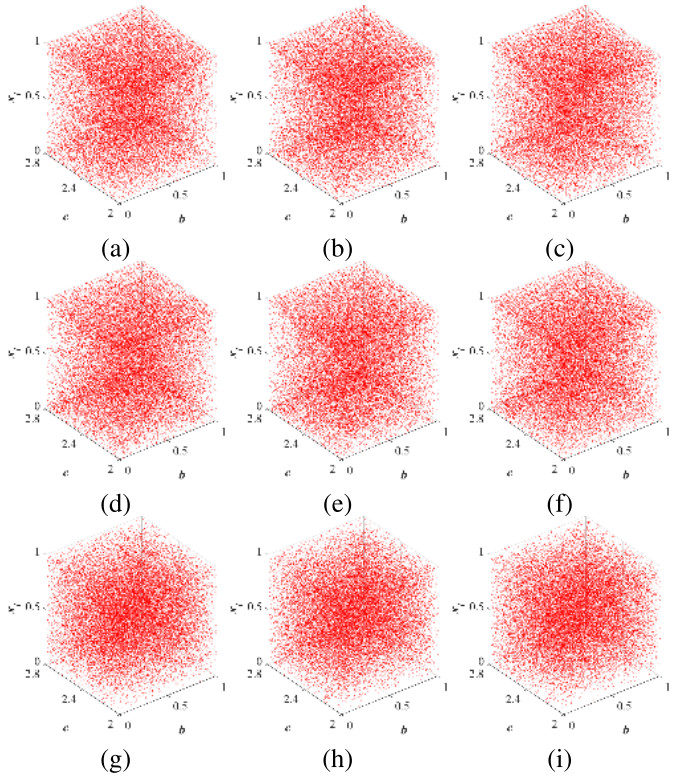

Fig. 3. Bifurcation diagrams of the chaotic maps of ECM on the parameter (b, c) space when $a = 1$. (a) LEL map. (b) LES map. (c) LET map. (d) SEL map. (e) SES map. (f) SET map. (g) TEL map. (h) TES map. (i) TET map.

A. Bifurcation Diagram

The bifurcation diagram of a dynamical system can occupy a portion of its phase space. A lower degree of density in the bifurcation diagram indicates more uniform chaotic signals of the corresponding dynamical system. Thus, the bifurcation diagram can visually reflect the behavior of a dynamical system.

Fig. 3 shows the bifurcation diagrams of these nine chaotic maps of ECM on the parameter (b, c) space, where $b \in [0, 1]$ and $c \in [2, 2.8]$. One can observe that these nine chaotic maps display complex chaotic behaviors in all the parameter settings. Their output values uniformly distribute in the whole output ranges. On the other hand, their base and exponent maps have chaotic behaviors only in small parameter ranges and their outputs cannot uniformly distribute, which can be observed from their bifurcation diagrams in Fig. 1. With uniform-distribution outputs, these new chaotic maps are suitable for many applications such as pseudo-random number generator.

A bifurcation structure can indicate how a dynamical system leads to chaos. As can be observed from Fig. 1, the existing logistic and sine maps have period-doubling bifurcation structures while the tent map has double-sided bifurcation structure leading to chaos. Because the proposed ECM is an efficient chaotification structure, the new chaotic maps produced by ECM have robust chaotic behaviors in the entire parameter space and they may not have obvious bifurcation structures that lead to chaos. Their robust chaos will be theoretically proved in the next section and experimentally analyzed using the LE and CD in Figs. 5 and 6.

B. Robust Chaos

According to Section II-B, the robust chaos is explained as the absence of periodic windows and coexisting attractors in the neighborhood of parameter space. This section proves that the nine chaotic maps of ECM in Table I can satisfy the requirements of robust chaos in parameter $b \in (0, 1)$ when parameters $a = 1$ and $c = 2.8$. As the LEL, LES, SEL, and SES maps are differentiable, we first use Theorem 1 to prove their robust chaos.

Lemma 1: The LEL, LES, SEL, and SES maps on $I = [0, 1] \to I$ are S-unimodal maps under the parameter $b \in (0, 1)$ when $a = 1$ and $c = 2.8$.

Proof: The LEL, LES, SEL, and SES maps in Table I are of class C^3, because their third derivatives exist and are continuous. Then condition 1 of Definition 1 is satisfied.

The LEL, LES, SEL, and SES maps satisfy that $\mathcal{E}(0) = \mathcal{E}(1) = 0$, as their base maps, the logistic map $L(r, x)$ and sine map $S(r, x)$ have $L(r, 0) = L(r, 1) = S(r, 0) = S(r, 1) = 0$. Then condition 2 of Definition 1 is satisfied.

Next, we investigate the extreme values of the LEL, LES, SEL, and SES maps under the parameter settings $b \in (0, 1)$, $a = 1$, and $c = 2.8$. The derivatives of the logistic map $L(r, x)$ and sine map $S(r, x)$ are calculated as

$$L'(r, x) = 4r(1 - 2x) \quad \text{and} \quad S'(r, x) = r\cos(\pi x)\pi. \tag{7}$$

Both $L(r, x)$ and $S(r, x)$ have unique maximums at $x = 0.5$ on $(0, 1)$. For $\forall r \in (0, 1)$, one can get

$$\begin{aligned} &L'(r, 0.5) = S'(r, 0.5) = 0 \\ &L'(r, x), S'(r, x) > 0 \quad \text{for} \quad 0 < x < 0.5 \\ &L'(r, x), S'(r, x) < 0 \quad \text{for} \quad 0.5 < x < 1. \end{aligned} \tag{8}$$

According to the calculation in (6), the derivative of ECM at $x = 0.5$ can be obtained as

$$J(0.5) = f(1, 0.5)^{\ln(g(b,0.5)+2.8)} \left(\frac{f'(1, 0.5)\ln(g(b, 0.5) + 2.8)}{f(1, 0.5)} + \frac{g'(b, 0.5)\ln(f(1, 0.5))}{g(b, 0.5) + 2.8} \right).$$

One can obtain that $f'(1, 0.5) = g'(b, 0.5) = 0$, because the base map $f(1, x)$ and exponent map $g(b, x)$ in the LEL, LES, SEL, and SES maps are the $L(r, x)$ or $S(r, x)$. Then

$$J(0.5) = 0. \tag{9}$$

When $0 < x < 1$, $f(1, x)^{\ln(g(b,x)+2.8)} > 0$. This is because $f(1, x)$ and $g(b, x)$ are $L(r, x)$ or $S(r, x)$, and $0 < L(r, x), S(r, x) < 1$. Then the sign of $J(x)$ in (6) is the same with that of the following equation:

$$\begin{aligned} \Delta = {} & f'(1, x)(g(b, x) + 2.8)\ln(g(b, x) + 2.8) \\ & + g'(b, x)f(1, x)\ln(f(1, x)). \end{aligned} \tag{10}$$

Let the function $H(x) = x\ln(x)$. One can get that

$$H'(x) = 1 + \ln(x).$$

$H'(x) < 0$ when $0 < x < (1/e)$; $H'(x) > 0$ when $x > (1/e)$; and $H'(1/e) = 0$. Then the minimum of $H(x)$ is $H(1/e) = -(1/e)$.

When $0 < x < 0.5$, $f(1,x)$, and $g(b,x)$ satisfy that $0 < f(1,x), g(b,x) < 1$, because they are the $L(r,x)$ or $S(r,x)$ and $0 < L(r,x), S(r,x) < 1$. Then one can obtain that

$$(g(b,x)+2.8)\ln(g(b,x)+2.8) > 2.8\ln 2.8 > 2.8$$
$$f(1,x)\ln(f(1,x)) \geq \frac{1}{e}\ln\left(\frac{1}{e}\right) = -\frac{1}{e}. \quad (11)$$

From (8), one can get that $f'(1,x), g'(b,x) > 0$ when $0 < x < 0.5$. Then Δ in (10) satisfies that

$$\Delta > 2.8\, f'(1,x) - \frac{1}{e}g'(b,x) = \delta(x).$$

As the base map $f(1,x)$ and exponent map $g(b,x)$ are logistic map $L(r,x)$ or sine map $S(r,x)$, the $\delta(x)$ for the LEL, LES, SEL, and SES maps when $0 < x < 0.5$ are obtained as

$$\delta_{\mathrm{LEL}}(x) = 2.8 \times 4(1-2x) - \frac{1}{e} \times 4b(1-2x) > 0$$
$$\delta_{\mathrm{SES}}(x) = 2.8 \times \cos(\pi x)\pi - \frac{1}{e} \times b\cos(\pi x)\pi > 0$$
$$\delta_{\mathrm{LES}}(x) = 2.8 \times 4(1-2x) - \frac{1}{e} \times b\cos(\pi x)\pi$$
$$\delta_{\mathrm{SEL}}(x) = 2.8 \times \cos(\pi x)\pi - \frac{1}{e} \times 4b(1-2x).$$

The derivative of $\delta_{\mathrm{LES}}(x)$ satisfies that $\delta'_{\mathrm{LES}}(x) < 0$ when $0 < x < 0.5$. Thus,

$$\delta_{\mathrm{LES}}(x) > \delta_{\mathrm{LES}}(0.5) = 0.$$

The derivative of $\delta_{\mathrm{SEL}}(x)$ can be calculated as

$$\delta'_{\mathrm{SEL}}(x) = -2.8\pi^2\sin(\pi x) + \frac{8b}{e}.$$

One can easily calculate out that when $0 < x < 0.5$, only one root $\hat{x}$ exists in $\delta'_{\mathrm{SEL}}(x) = 0$ and $\delta'_{\mathrm{SEL}}(0) > 0$. Thus, $\delta_{\mathrm{SEL}}(x)$ strictly increases on $x \in (0, \hat{x}]$, and strictly decreases on $x \in [\hat{x}, 0.5)$. Then

$$\delta_{\mathrm{SEL}}(x) > \min\{\delta_{\mathrm{SEL}}(0), \delta_{\mathrm{SEL}}(0.5)\} = 0.$$

Thus, we can obtain that when $0 < x < 0.5$, the Δ of the LEL, LES, SEL, and SES maps have $\Delta = \delta(x) > 0$. Because the sign of $J(x)$ is the same with that of the Δ, one can obtain that

$$J(x) > 0 \quad \text{for} \quad 0 < x < 0.5. \quad (12)$$

When $0.5 < x < 1$, one can get that $g'(b,x), f'(1,x) < 0$ from (8). Using (11), the Δ in (10) satisfies that

$$\Delta < 2.8\, f'(1,x) - \frac{1}{e}g'(b,x).$$

Using the same analysis with $0 < x < 0.5$, we can obtain

$$J(x) < 0 \quad \text{for} \quad 0.5 < x < 1. \quad (13)$$

Combining (9), (12), and (13), one can get that the LEL, LES, SEL, and SES maps have unique local maximums at $x = 0.5$ on $(0,1)$. Then condition 3 of Definition 1 is satisfied.

The Schwarzian derivative of ECM is defined as

$$S(\mathcal{E},x) = \frac{\mathcal{E}'''(x)}{\mathcal{E}'(x)} - \frac{3}{2}\left(\frac{\mathcal{E}''(x)}{\mathcal{E}'(x)}\right)^2.$$

According to the definitions of the LEL, LES, SEL, and SES maps in Table I, one can calculate that when $a = 1$ and $c = 2.8$, the Schwarzian derivatives of the LEL, LES, SEL, and SES maps on $x \in [0,1]$ are negative for parameter $b \in [0,1]$ except for the maximum point at $x = 0.5$. Then condition 4 of Definition 1 is satisfied. Thus, all conditions of Definition 1 are satisfied and the LEL, LES, SEL, and SES maps are S-unimodal maps on $I = [0,1] \to I$ under $b \in (0,1)$ when $a = 1$ and $c = 2.8$. ■

Lemma 2: The LEL, LES, SEL, and SES maps on $I = [0,1] \to I$ can generate robust chaos for parameter $b \in (0,1)$ when $a = 1$ and $c = 2.8$.

Proof: Lemma 1 has stated that the LEL, LES, SEL, and SES maps are S-unimodal maps on $I = [0,1] \to I$. From (9), (12), and (13), one can get that the LEL, LES, SEL, and SES maps have unique maximums at $x = 0.5$ for $\forall b \in (0,1)$. When $a = 1$, the maximums of the four chaotic maps can be obtained as $\mathcal{E}^{\max}_{\mathrm{LEL}}(0.5) = \mathcal{E}^{\max}_{\mathrm{LES}}(0.5) = \mathcal{E}^{\max}_{\mathrm{SEL}}(0.5) = \mathcal{E}^{\max}_{\mathrm{SES}}(0.5) = 1$ for $\forall b \in (0,1)$. This is because their base maps, the logistic map $L(r,x)$ and sine map $S(r,x)$ satisfy that $L(1,0.5) = S(1,0.5) = 1$. Thus, Theorem 1 is satisfied and the LEL, LES, SEL, and SES maps on $I = [0,1] \to I$ can generate robust chaos for $b \in (0,1)$ when $a = 1$ and $c = 2.8$. ■

As the LET, SET, TEL, TES, and TET maps are piecewise maps and are not differentiable, one cannot use Theorem 1 to analyze their robust chaos. However, their robust chaotic behaviors can be analyzed using the stability of their fixed points. Using (5) and (6), one can calculate out all fixed points and the related derivatives of these chaotic maps listed in Table I. Fig. 4 plots the calculated fixed points and the related derivatives of these chaotic maps on parameter space $b \in (0,1)$ when $a = 1$ and $c = 2.8$. As can be seen, these nine chaotic maps have unique fixed points on $(0,1)$ and their related absolute derivatives $|J| > 1$ for the whole parameter space $b \in (0,1)$. Thus, all the nine chaotic maps do not have stable periodic orbits and they own unique chaotic attractors in the whole parameter space b, indicating that they have robust chaotic behaviors.

V. Performance Evaluations

This section quantitatively evaluates the nine chaotic maps of ECM in the parameter (b,c) space. The chaotic behaviors are evaluated using the LE [40], CD [43], and initial state sensitivity.

A. Lyapunov Exponent

The LE is a commonly used criterion to test the existence of chaos [40]. It can test the chaos of a dynamical system from the deterministic equation(s). For two trajectories of a dynamical system starting from extremely close initial states, the LE measures their average separation rate in every unit time. Mathematically, the LE of the dynamical system

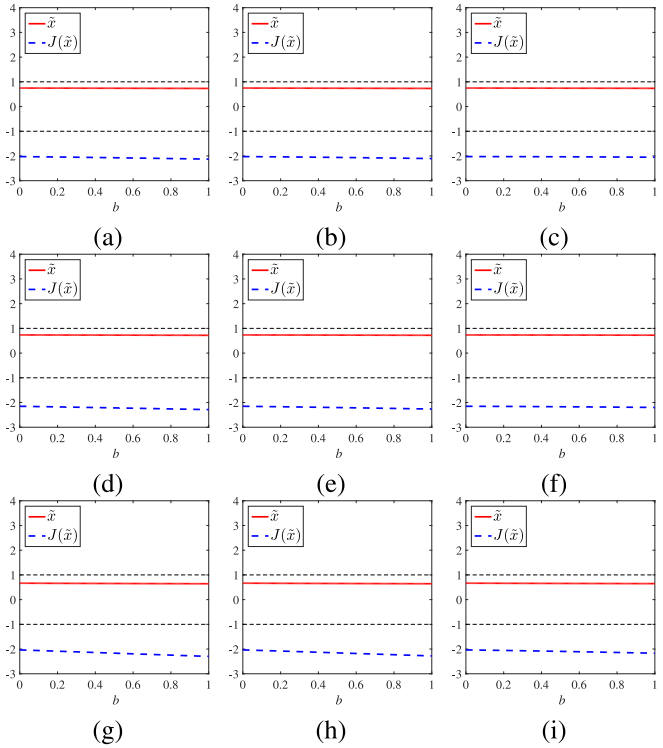

Fig. 4. Fixed points $\tilde{x}$ and their related derivatives $J(\tilde{x})$ of the nine chaotic maps of ECM. (a) LEL map. (b) LES map. (c) LET map. (d) SEL map. (e) SES map. (f) SET map. (g) TEL map. (h) TES map. (i) TET map.

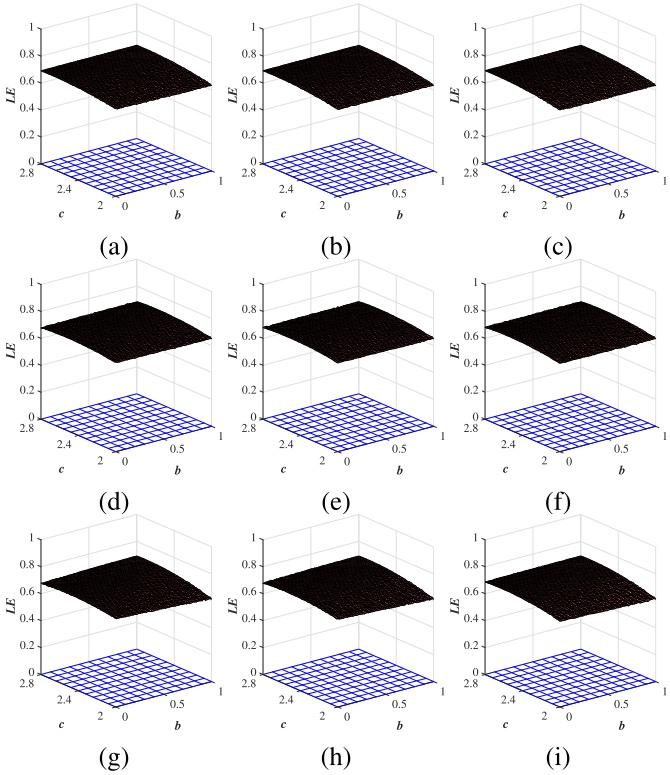

Fig. 5. LEs of the chaotic maps produced by ECM on the parameter (b, c) space. (a) LEL map. (b) LES map. (c) LET map. (d) SEL map. (e) SES map. (f) SET map. (g) TEL map. (h) TES map. (i) TET map.

$x_{i+1} = \mathcal{F}(x_i)$ is defined as

$$\lambda_{\mathcal{F}(x)} = \lim_{n\to\infty}\left\{\frac{1}{n}\ln\left|\frac{\mathcal{F}^n(x_0+\varepsilon)-\mathcal{F}^n(x_0)}{\varepsilon}\right|\right\} \tag{14}$$

where ε indicates a very small positive quantity. If $\mathcal{F}(\cdot)$ is differentiable, its LE can also be defined as

$$\lambda_{\mathcal{F}(x)} = \lim_{n\to\infty}\left\{\frac{1}{n}\sum_{i=0}^{n-1}\ln\left|\mathcal{F}'(x_i)\right|\right\}. \tag{15}$$

A positive LE demonstrates that small changes in the dynamical system's initial states can lead to completely different behaviors. Thus, one positive LE is an indicator of chaotic behaviors if some other conditions (e.g., phase space compactness) also meet [44]. A bigger positive LE means a faster separation rate.

Our experiment uses the definition of LE to estimate the LEs of different chaotic maps. When estimating the LEs, the first 100 iteration values of the chaotic maps are discarded. Fig. 5 plots the computed LEs of the chaotic maps in Table I with respect to parameters $b \in [0, 1]$ and $c \in [2, 2.8]$ when $a = 1$. The step sizes for b and c are 0.016 and 0.02, respectively. One can see that the nine chaotic maps have positive LEs in all the parameter (b, c) space, and their chaotic ranges are continuous. On the other hand, their base and exponent maps have positive LEs in only small chaotic ranges that are discontinuous. These can be seen in Fig. 1. This indicates that these chaotic maps produced by ECM have robust chaotic behaviors in a large parameter space of b and c.

B. Correlation Dimension

The CD is a type of fractal dimension. It is a metric to measure the space dimensionality occupied by a time series [43]. Different from the LE that tests the chaos from the deterministic equation(s), the CD can test the existence of chaos from experimental data. For an embedding dimension e and a time series $\{S_i | i = 1, 2, \ldots, N\}$ generated by a chaotic system, the CD is defined as

$$\mathrm{CD} = \lim_{r\to 0}\lim_{N\to\infty}\frac{\log C_e(r)}{\log r} \tag{16}$$

where $C_e(r)$ is the correlation integral that is defined by

$$C_e(r) = \lim_{N\to\infty}\frac{1}{[N-(e-1)\ell][N-(e-1)\ell-1]} \times \sum_{i=1}^{N-(e-1)\ell}\sum_{j=i+1}^{N-(e-1)\ell}\theta\left(r-|\bar{S}_i-\bar{S}_j|\right) \tag{17}$$

where $\theta(\alpha)$ is a step function. $\theta(\alpha) = 1$ if $\alpha \geq 0$ and $\theta(\alpha) = 0$ if $\alpha < 0$. ℓ is the time delay unit and it usually equals to 1 for discrete-time system. The new time series $\{\bar{S}_t | t = 1, 2, 3, \ldots, \}$ is derived from $\{S_i | i = 1, 2, \ldots, N\}$ and is represented as

$$\bar{S}_t = \left(S_t, S_{t+\ell}, S_{t+2\ell}, \ldots, S_{t+(e-1)\ell}\right)$$
$$t \in \{1, 2, \ldots, N-(e-1)\ell\}.$$

If it exists, the CD can also be presented as the gradient of $\log C_e(r)$ against $\log r$, namely

$$\mathrm{CD} = \lim_{r\to 0}\lim_{N\to\infty}\frac{d(\log C_e(r))/dr}{d(\log r)/dr}. \tag{18}$$

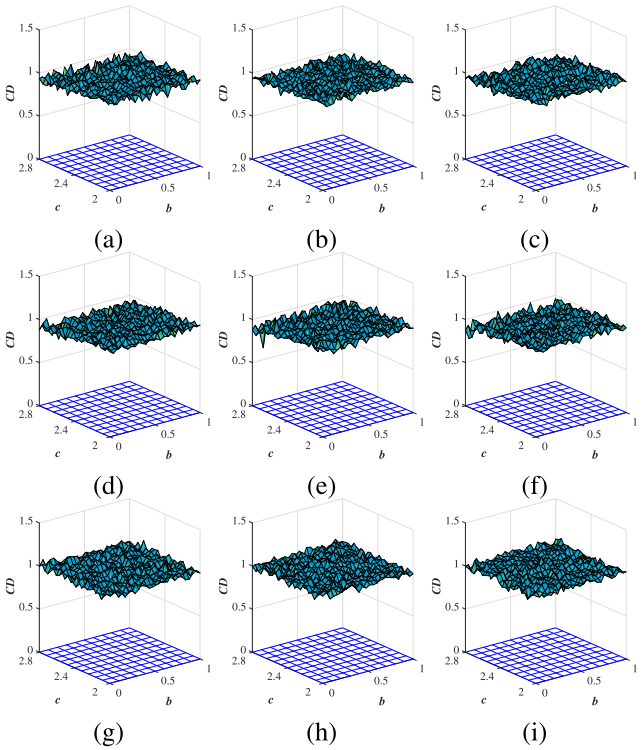

Fig. 6. CDs of the chaotic maps produced by ECM on the parameter (b, c) space. (a) LEL map. (b) LES map. (c) LET map. (d) SEL map. (e) SES map. (f) SET map. (g) TEL map. (h) TES map. (i) TET map.

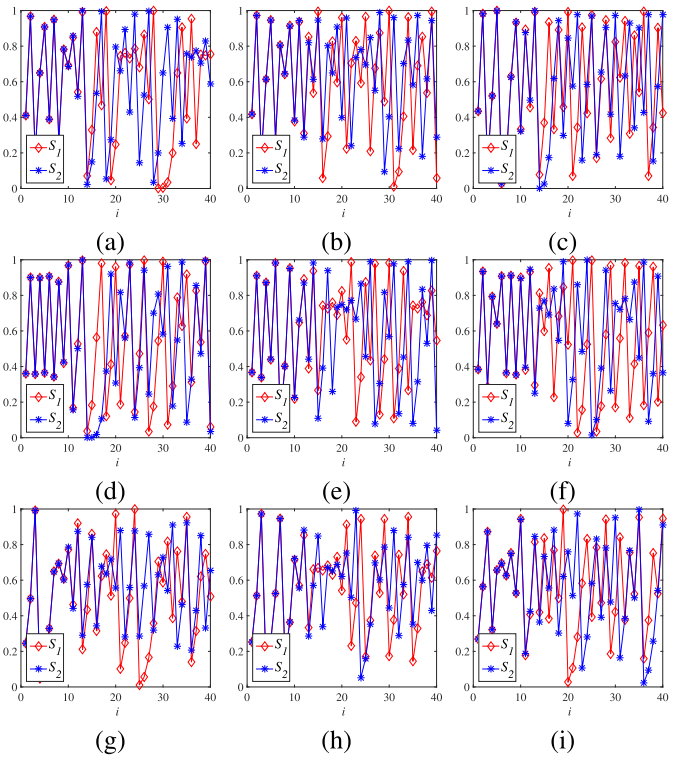

Fig. 7. Chaotic trajectories S_1 and S_2, which are generated using initial states $(x_0, b, c) = (0.1, 0.8, 2.1)$ and $(x_0, b, c) = (0.10001, 0.8, 2.1)$, respectively. (a) LEL map. (b) LES map. (c) LET map. (d) SEL map. (e) SES map. (f) SET map. (g) TEL map. (h) TES map. (i) TET map.

A bigger CD indicates that a dynamical system can generate outputs occupying a larger dimensionality and thus its attractors are more irregular.

Our experiments use the Grassberger–Procaccia algorithm [45] to compute the CDs of time series generated by different chaotic maps and Fig. 6 shows the computed CDs of the nine chaotic maps with respect to parameters $b \in [0, 1]$ and $c \in [2, 2.8]$ when $a = 1$. The step sizes for b and c are 0.032 and 0.04, respectively. One can see that the chaotic maps of ECM have positive CDs in all the parameter space of b and c. The experimental results are consistent with the LE results. This means that the chaotic maps of ECM have robust chaotic behaviors from the viewpoints of experimental data.

C. Initial State Sensitivity

The most important and straightforward property of the "chaos" is the initial state sensitivity [46], which means that a dynamical system owing chaotic behaviors is sensitive to the change of its control parameter(s) and initial value. The initial state sensitivity can be measured using the correlation coefficient (CC), which is defined as

$$\mathrm{CC}(X, Y) = \frac{E[(X_t - \mu_X)(Y_t - \mu_Y)]}{\sigma_X \sigma_Y} \tag{19}$$

where X_t and Y_t are two sequences of data, μ is the mean value, σ is the standard deviation, and $E[.]$ is the expectation function. The absolute CC closing to 1 means that the data sequences X_t and Y_t have high relationship, and vice versa.

For each of the nine chaotic maps produced by ECM, our experiments are designed as follows.

1) Generate a chaotic trajectory S_1 of length 50 000 using the initial state $(x_0, b, c) = (0.1, 0.8, 2.1)$.
2) Generate other three chaotic trajectories S_2, S_3, and S_4 of length 50 000. The used initial states have small changes with the initial state of generating S_1. Specifically, the initial states for generating S_2, S_3, and S_4 are $(x_0, b, c) = (0.10001, 0.8, 2.1)$, $(x_0, b, c) = (0.1, 0.80001, 2.1)$, and $(x_0, b, c) = (0.1, 0.8, 2.10001)$, respectively.
3) Calculate the correlation coefficient $CC(S_1, S_2)$, $CC(S_1, S_3)$, and $CC(S_1, S_4)$. Fig. 7 plots the first 40 states of chaotic trajectories S_1 and S_2 and Fig. 8 plots the differences between S_3 and S_1, and between S_4 and S_1 in the first 40 states. As can be seen, when the iteration increases, the small change in the initial value or control parameters can result in significantly different outputs. Table II shows the CCs of the nine chaotic maps produced by ECM. One can see that all the CCs approach to 0. These prove that the chaotic maps of ECM are quite sensitive to their initial states.

VI. Application to Secure Communication

Chaos is a natural candidate for secure communication, due to its significant properties, such as the unpredictability and ergodicity [47]. When chaotic maps are applied to secure communication, the distribution of their chaotic signals greatly affects the performance of resisting channel noise. As the chaotic maps produced by ECM have uniformly distributed chaotic signals, they are suitable for secure communication.

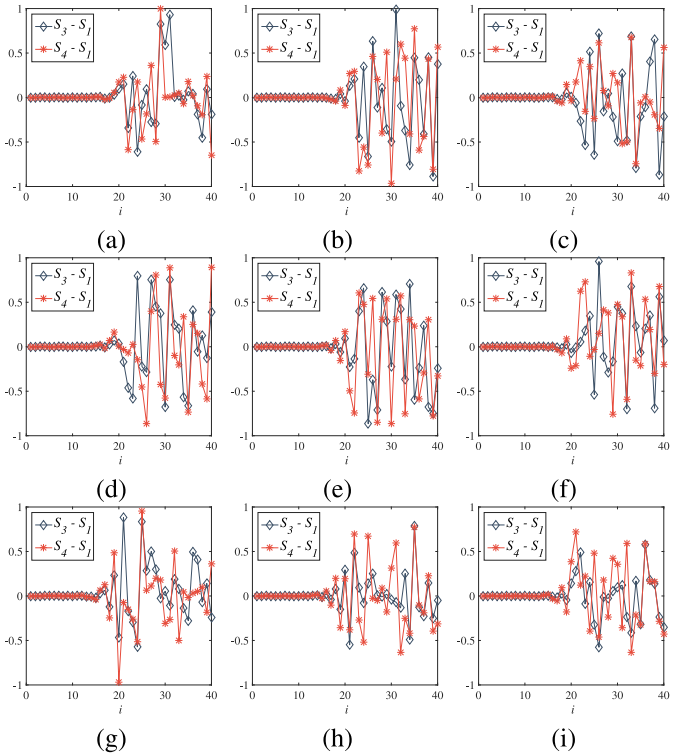

Fig. 8. Differences between S_3 and S_1, and between S_4 and S_1. The chaotic trajectories S_1, S_3, and S_4 are generated using initial states $(x_0, b, c) = (0.1, 0.8, 2.1)$, $(x_0, b, c) = (0.1, 0.80001, 2.1)$, and $(x_0, b, c) = (0.1, 0.8, 2.10001)$, respectively. (a) LEL map. (b) LES map. (c) LET map. (d) SEL map. (e) SES map. (f) SET map. (g) TEL map. (h) TES map. (i) TET map.

TABLE II
CCs OF CHAOTIC TRAJECTORIES OF THE NINE NEW CHAOTIC MAPS

Chaotic maps	$CC(S_1, S_2)$	$CC(S_1, S_3)$	$CC(S_1, S_4)$
LEL map	0.0079	-0.0077	-0.0032
LES map	-0.0060	0.0058	0.0047
LET map	-0.0084	0.0050	-0.0048
SEL map	-0.0053	-0.0083	0.0012
SES map	0.0039	-0.0003	-0.0077
SET map	-0.0064	-0.0083	-0.0137
TEL map	0.0009	-0.0026	0.0084
TES map	-0.0030	0.0047	0.0049
TET map	-0.0022	-0.0006	0.0011

Here, we use the reference-shifted differential chaos shift keying (RS-DCSK) [48] to demonstrate the application of the chaotic maps generated by ECM in secure communication.

A. RS-DCSK

The RS-DCSK is a kind of noncoherent frameworks [47] and it is able to recover the information bits using the inner correlation of the received signal. It can be divided into two parts: 1) the transmitter and 2) receiver. The transmitter is to encode the information bits using chaotic sequences and sends the transmission signal to the receiver, while the receiver decodes the received signal to recover the information bits.

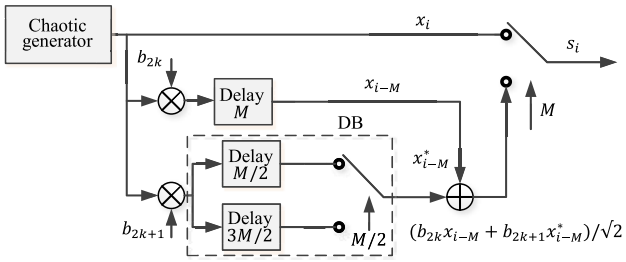

Fig. 9. Transmitter of the RS-DCSK.

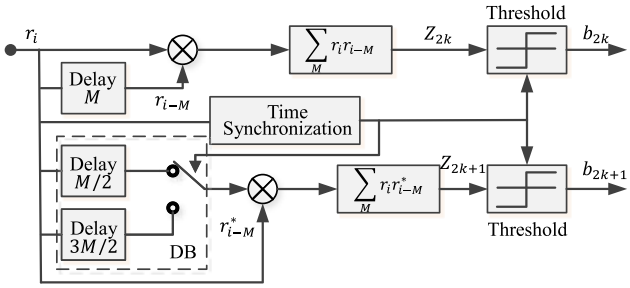

Fig. 10. Receiver of the RS-DCSK.

1) Transmitter: Fig. 9 shows the structure of the transmitter in RS-DCSK. The signal is transmitted frame by frame. A frame consists of two parts: 1) reference signal and 2) information signal. Suppose the spread factor is M, the reference signal is an M-length chaotic sequence generated by a chaotic generator, while the information signal is obtained by modifying the reference signal using the information bits. As can be seen from Fig. 9, the kth frame contains two information bits, b_{2k} and b_{2k+1}. The information signal for b_{2k} is $\{x_{2kM+1}, \ldots, x_{2(k+1)M}\}$, while the information signal for b_{2k+1} is $\{x_{(2k+1/2)M+1}, x_{(2k+1/2)M+2}, \ldots, x_{2(k+1)M}, x_{2kM+1}, \ldots, x_{(2k+1/2)M}\}$, which is obtained by circularly shifting the reference signal of b_{2k} by $M/2$. Subsequently, the reference signal and information signal are modulated to obtain the transmission signal s_i. In summary, the kth frame of the transmission signal $s_i(k)$ can be obtained by the following equation:

$$s_i(k) = \begin{cases} x_i & \text{for } 2kM < i \le (2k+1)M \\ \frac{b_{2k}x_{i-M} + b_{2k+1}x_{i-M/2}}{\sqrt{2}} & \text{for } (2k+1)M < i \le \left(2k+\frac{3}{2}\right)M \\ \frac{b_{2k}x_{i-M} + b_{2k+1}x_{i-3M/2}}{\sqrt{2}} & \text{for } \left(2k+\frac{3}{2}\right)M < i \le (2k+2)M. \end{cases} \tag{20}$$

2) Receiver: The receiver is to recover the information bits and it is shown in Fig. 10. Because a signal may be blurred by channel noise during transmission, the received signal is different from the original transmission signal and it can be described as $r_i = s_i + \xi_i$, where ξ_i is the noise. To recover the information bits, the received signal r_i is multiplied with its delayed signal r_{i-M} and r^*_{i-M}. The signal r^*_{i-M} is obtained by circularly shifting r_{i-M} for $M/2$. Then two correlators can be

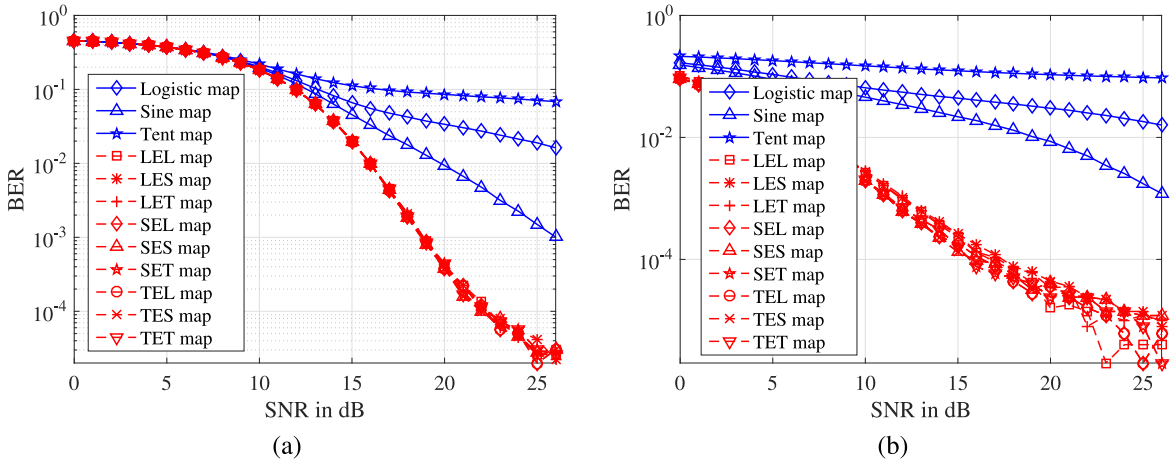

Fig. 11. BERs of the RS-DCSK using different chaotic maps under various signal-noise-rates (SNRs) in the (a) AWGN channel and (b) ARN channel.

calculated as [48]

$$Z_{2k} = \sum_{i=(2k+1)M+1}^{2(k+1)M} r_{i-M} r_i = \frac{b_{2k}}{\sqrt{2}} \sum_{i=(2k+1)M+1}^{2(k+1)M} x_{i-M}^2 + \gamma \tag{21}$$

$$Z_{2k+1} = \sum_{i=(2k+1)M+1}^{2(k+1)M} r_{i-M}^* r_i = \frac{b_{2k+1}}{\sqrt{2}} \sum_{i=(2k+1)M+1}^{2(k+1)M} x_{i-M}^2 + \eta \tag{22}$$

where γ and η are noise components. As the energy of noise component is far smaller than the energy of the transmission signal s_i, the symbols of Z_{2k} and Z_{2k+1} are determined by the information components, namely $(b_{2k}/\sqrt{2}) \sum_{i=(2k+1)M+1}^{2(k+1)M} x_{i-M}^2$ and $(b_{2k+1}/\sqrt{2}) \sum_{i=(2k+1)M+1}^{2(k+1)M} x_{i-M}^2$, respectively. The obtained Z_i is a positive number if the information bit is "1"; and Z_i is a negative number if the information bit is "-1". Thus, despite the noise components, the two information bits b_{2k} and b_{2k+1} can be recovered by

$$\hat{b}_n = \begin{cases} 1 & \text{for} \quad Z_n > 0 \\ -1 & \text{for} \quad Z_n \leq 0. \end{cases} \tag{23}$$

B. Simulation Results

When data are transmitted in noisy transmission channels, the additive white Gaussian noise (AWGN) and additive random noise (ARN) are frequently encountered. Thus, we simulate the RS-DCSK in the AWGN and ARN channels under different lengths of the spread factor. The bit error rate (BER) between the original data and recovered data is investigated to demonstrate the ability of resisting noise. The chaotic generator is selected as the nine chaotic maps of ECM in Table I and their base and exponent maps, respectively. The original information in each simulation is a randomly generated sequence with a 50 000-bit length.

TABLE III
CHAOTIC RANGES AND STEP SIZES FOR DIFFERENT CHAOTIC MAPS IN OUR EXPERIMENTS

Chaotic maps	Chaotic ranges	Step sizes
Logistic map	$r \in (0.89, 1]$	$I_r = 0.011$
Sine map	$r \in (0.87, 1]$	$I_r = 0.013$
Tent map	$r \in (0.5, 0.99]$	$I_r = 0.049$
LEL, LES, LET, SEL, SES, SET, TEL, TES and TET maps	$b \in (0, 1]$ $c \in (2, 2.8]$	$I_b = 0.1$ $I_c = 0.08$

We design two groups of experiments to test the BERs of RS-DCSK using different chaotic maps as the chaotic generator. The first group of experiments investigates the BERs against different levels of noise. The experiments for each chaotic map are set as follows.

1) Generate ten initial states. The initial value is set as $x_0 = 0.2$ and the ten control parameters are obtained from the chaotic range. Specifically, for a chaotic range (C_1, C_2) with a step size I, the mth control parameter is $C_1 + mI$. Table III lists the used chaotic ranges and step sizes for all the chaotic maps.
2) Set the length of the spread factor $M = 40$ and then simulate the RS-DCSK ten times using the ten initial states, and obtain the BERs in different levels of AWGN and ARN.
3) Calculate the average BERs of the ten times of experiments. Fig. 11 shows the average BERs of RS-DCSK using different chaotic maps in different levels of AWGN and ARN.

The second group of experiments investigates the BERs against different lengths of the spread factor M. The experiments for each chaotic map are set as follows.

1) Generate ten initial states using the same way as the first group of experiments.
2) Set the channel noise AWGN and ARN as 18 dB and then simulate the RS-DCSK ten times using the ten

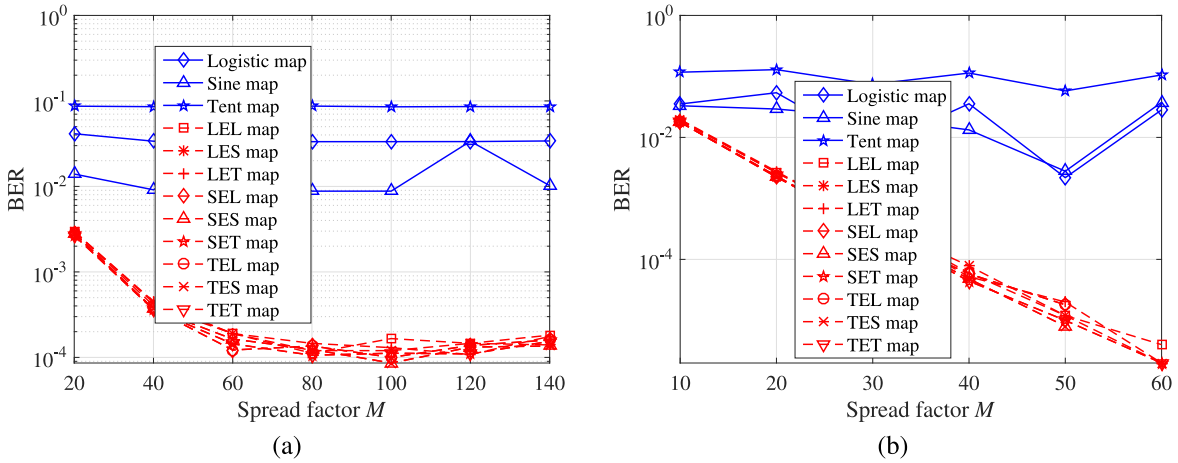

Fig. 12. BERs of the RS-DCSK using different chaotic maps under various lengths of the spread factor M in the (a) AWGN channel and (b) ARN channel.

initial states, and obtain the BERs under different lengths of the spread factor.

3) Calculate the average BERs of the ten times of experiments. Fig. 12 shows the average BERs of RS-DCSK using different chaotic maps under different lengths of the spread factor M.

Fig. 11 shows that, with the increment of SNR in both AWGN and ARN channels, the RS-DCSK using the nine chaotic maps of ECM can obtain much smaller BERs than that of using the logistic, sine, and tent maps. Fig. 12 shows that, under various lengths of the spread factor, the RS-DCSK using the nine chaotic maps of ECM can always achieve much smaller BERs than that of using the three existing chaotic maps. This is because the nine chaotic maps generated by ECM can output much more uniform-distribution chaotic signals than the logistic, sine, and tent maps, as shown in Figs. 1 and 3. The transmission signals can achieve stronger ability of resisting channel noise if the used chaotic signals distribute more uniformly. As a result, the chaotic maps of ECM exhibit high performance in secure communication.

VII. Conclusion

Robust chaos is a desired property for many chaos-based applications. However, existing chaotic systems may not own this property. To address this issue, this article introduced an ECM to obtain new 1-D chaotic maps with robust chaos. Motivated by the nonlinear property of exponential operation in arithmetic, ECM employs two chaotic maps as base and exponent maps to produce new chaotic maps. To show the effectiveness of ECM, we used three existing chaotic maps as the base and exponent maps to produce nine new chaotic maps as examples. Theoretical analysis verified that these new chaotic maps can generate robust chaos. Performance evaluations using LE, CD, and CC demonstrated that the nine chaotic maps of ECM are sensitive to their initial states, and have robust chaotic behaviors. To show ECM in real applications, we applied the nine chaotic maps of ECM as chaotic generators in secure communication. The simulation results showed that these new chaotic maps exhibit better performance in resisting channel noise than their base and exponent maps. Our future work will investigate the robust chaos of high-dimensional chaotic systems and the application of robust chaos in pseudo-random number generator.

Acknowledgment

The authors would like to thank the anonymous reviewers for their valuable comments and suggestions that greatly contribute to improving the quality of this article.

References

[1] Y. Huang, Q. Huang, and Q. Wang, "Chaos and bifurcation control of torque-stiffness-controlled dynamic bipedal walking," *IEEE Trans. Syst., Man, Cybern., Syst.*, vol. 47, no. 7, pp. 1229–1240, Jul. 2017.

[2] E. N. Lorenz, "Deterministic nonperiodic flow," *J. Atmos. Sci.*, vol. 20, no. 2, pp. 130–141, 1963.

[3] S. Vaidyanathan and C. Volos, *Advances and Applications in Chaotic Systems*. Berlin, Germany: Springer, 2016.

[4] H. Bao, A. Hu, W. Liu, and B. Bao, "Hidden bursting firings and bifurcation mechanisms in memristive neuron model with threshold electromagnetic induction," *IEEE Trans. Neural Netw. Learn. Syst.*, to be published.

[5] R. L. Devaney, *An Introduction to Chaotic Dynamical Systems*, 2nd ed. Boulder, CO, USA: Westview, 2003.

[6] Z. Hua, B. Zhou, and Y. Zhou, "Sine-transform-based chaotic system with FPGA implementation," *IEEE Trans. Ind. Electron.*, vol. 65, no. 3, pp. 2557–2566, Mar. 2018.

[7] L. Yin, Z. Deng, B. Huo, and Y. Xia, "Finite-time synchronization for chaotic gyros systems with terminal sliding mode control," *IEEE Trans. Syst., Man, Cybern., Syst.*, vol. 49, no. 6, pp. 1131–1140, Jun. 2019.

[8] C. Li, D. Lin, J. Lü, and F. Hao, "Cryptanalyzing an image encryption algorithm based on autoblocking and electrocardiography," *IEEE MultiMedia*, vol. 25, no. 4, pp. 46–56, Oct./Dec. 2018.

[9] M. Chen, M. Sun, H. Bao, Y. Hu, and B. Bao, "Flux-charge analysis of two-memristor-based Chua's circuit: Dimensionality decreasing model for detecting extreme multistability," *IEEE Trans. Ind. Electron.*, to be published.

[10] Z. Lin, S. Yu, J. Lü, S. Cai, and G. Chen, "Design and ARM-embedded implementation of a chaotic map-based real-time secure video communication system," *IEEE Trans. Circuits Syst. Video Technol.*, vol. 25, no. 7, pp. 1203–1216, Jul. 2015.

[11] S. Chen, S. Yu, J. Lü, G. Chen, and J. He, "Design and FPGA-based realization of a chaotic secure video communication system," *IEEE Trans. Circuits Syst. Video Technol.*, vol. 28, no. 9, pp. 2359–2371, Sep. 2018.

[12] Y. Zhang and D. Xiao, "Double optical image encryption using discrete Chirikov standard map and chaos-based fractional random transform," *Opt. Lasers Eng.*, vol. 51, no. 4, pp. 472–480, 2013.

[13] B. Chen, C. Lin, X. Liu, and K. Liu, "Observer-based adaptive fuzzy control for a class of nonlinear delayed systems," *IEEE Trans. Syst., Man, Cybern., Syst.*, vol. 46, no. 1, pp. 27–36, Jan. 2016.

[14] B. Niu, C. K. Ahn, H. Li, and M. Liu, "Adaptive control for stochastic switched nonlower triangular nonlinear systems and its application to a one-link manipulator," *IEEE Trans. Syst., Man, Cybern., Syst.*, vol. 48, no. 10, pp. 1701–1714, Oct. 2018.
[15] V. Patidar, K. K. Sud, and N. K. Pareek, "A pseudo random bit generator based on chaotic logistic map and its statistical testing," *Informatica*, vol. 33, no. 4, pp. 441–452, 2009.
[16] S. H. Strogatz, *Nonlinear Dynamics and Chaos: With Applications to Physics, Biology, Chemistry, and Engineering*. Boulder, CO, USA: Westview, 2014.
[17] Y. Zhang, D. Xiao, Y. Shu, and J. Li, "A novel image encryption scheme based on a linear hyperbolic chaotic system of partial differential equations," *Signal Process. Image Commun.*, vol. 28, no. 3, pp. 292–300, 2013.
[18] J. M. Grzybowski, M. Eisencraft, and E. E. Macau, *Chaos-Based Communication Systems: Current Trends and Challenges*. Berlin, Germany: Springer, 2011, pp. 203–230.
[19] C. Li, B. Feng, S. Li, J. Kurths, and G. Chen, "Dynamic analysis of digital chaotic maps via state-mapping networks," *IEEE Trans. Circuits Syst. I, Reg. Papers*, vol. 66, no. 6, pp. 2322–2335, Jun. 2019.
[20] Z. Canyan, Z. Lihua, W. Yiming, L. Jiasheng, and M. Lingfeng, "Periodic performance of the chaotic spread spectrum sequence on finite precision," *J. Syst. Eng. Electron.*, vol. 19, no. 4, pp. 672–678, Aug. 2008.
[21] S. Ergün, "On the security of chaos based 'true' random number generators," *IEICE Trans. Fundam. Electron. Commun. Comput. Sci.*, vol. 99, no. 1, pp. 363–369, 2016.
[22] H. Zhao, S. Gao, Z. He, X. Zeng, W. Jin, and T. Li, "Identification of nonlinear dynamic system using a novel recurrent wavelet neural network based on the pipelined architecture," *IEEE Trans. Ind. Electron.*, vol. 61, no. 8, pp. 4171–4182, Aug. 2014.
[23] M. Han, R. Zhang, T. Qiu, M. Xu, and W. Ren, "Multivariate chaotic time series prediction based on improved grey relational analysis," *IEEE Trans. Syst., Man, Cybern., Syst.*, to be published.
[24] M. Han, K. Zhong, T. Qiu, and B. Han, "Interval type-2 fuzzy neural networks for chaotic time series prediction: A concise overview," *IEEE Trans. Cybern.*, vol. 49, no. 7, pp. 2720–2731, Jul. 2019.
[25] Z. Chen, X. Yuan, Y. Yuan, H. H.-C. Iu, and T. Fernando, "Parameter identification of chaotic and hyper-chaotic systems using synchronization-based parameter observer," *IEEE Trans. Circuits Syst. I, Reg. Papers*, vol. 63, no. 9, pp. 1464–1475, Sep. 2016.
[26] E. Zeraoulia, *Robust Chaos and Its Applications*, vol. 79. Singapore: World Sci., 2012.
[27] I. Sushko, L. Gardini, and K. Matsuyama, "Robust chaos in a credit cycle model defined by a one-dimensional piecewise smooth map," *Chaos Solitons Fractals*, vol. 91, pp. 299–309, Oct. 2016.
[28] S. P. Kuznetsov, "From geodesic flow on a surface of negative curvature to electronic generator of robust chaos," *Int. J. Bifurcation Chaos*, vol. 26, no. 14, 2016, Art. no. 1650232.
[29] R. Lan, J. He, S. Wang, Y. Liu, and X. Luo, "A parameter-selection-based chaotic system," *IEEE Trans. Circuits Syst. II, Exp. Briefs*, vol. 66, no. 3, pp. 492–496, Mar. 2019.
[30] Z. Hua, Y. Zhou, and H. Huang, "Cosine-transform-based chaotic system for image encryption," *Inf. Sci.*, vol. 480, pp. 403–419, Apr. 2019.
[31] Y. Deng, H. Hu, W. Xiong, N. N. Xiong, and L. Liu, "Analysis and design of digital chaotic systems with desirable performance via feedback control," *IEEE Trans. Syst., Man, Cybern., Syst.*, vol. 45, no. 8, pp. 1187–1200, Aug. 2015.
[32] C.-Y. Li, Y.-H. Chen, T.-Y. Chang, L.-Y. Deng, and K. To, "Period extension and randomness enhancement using high-throughput reseeding-mixing PRNG," *IEEE Trans. Very Large Scale Integr. (VLSI) Syst.*, vol. 20, no. 2, pp. 385–389, Feb. 2012.
[33] Y. Wu, Y. Zhou, and L. Bao, "Discrete wheel-switching chaotic system and applications," *IEEE Trans. Circuits Syst. I, Reg. Papers*, vol. 61, no. 12, pp. 3469–3477, Dec. 2014.
[34] Z. Hua, Y. Zhou, and B.-C. Bao, "Two-dimensional sine chaotification system with hardware implementation," *IEEE Trans. Ind. Informat.*, to be published.
[35] Y. Huang, P. Zhang, and W. Zhao, "Novel grid multiwing butterfly chaotic attractors and their circuit design," *IEEE Trans. Circuits Syst. II, Exp. Briefs*, vol. 62, no. 5, pp. 496–500, May 2015.
[36] C. Shen, S. Yu, J. Lü, and G. Chen, "Designing hyperchaotic systems with any desired number of positive Lyapunov exponents via a simple model," *IEEE Trans. Circuits Syst. I, Reg. Papers*, vol. 61, no. 8, pp. 2380–2389, Aug. 2014.
[37] X. Shen and Z. Jia, "On the existence structure of one-dimensional discrete chaotic systems," *J. Math. Res.*, vol. 3, no. 3, pp. 22–27, 2011.
[38] Z. Hua and Y. Zhou, "Dynamic parameter-control chaotic system," *IEEE Trans. Cybern.*, vol. 46, no. 12, pp. 3330–3341, Dec. 2016.
[39] Y. Zhou, Z. Hua, C.-M. Pun, and C. L. P. Chen, "Cascade chaotic system with applications," *IEEE Trans. Cybern.*, vol. 45, no. 9, pp. 2001–2012, Sep. 2015.
[40] A. Wolf, J. B. Swift, H. L. Swinney, and J. A. Vastano, "Determining Lyapunov exponents from a time series," *Physica D Nonlin. Phenom.*, vol. 16, no. 3, pp. 285–317, 1985.
[41] N. Nagaraj, M. C. Shastry, and P. G. Vaidya, "Increasing average period lengths by switching of robust chaos maps in finite precision," *Eur. Phys. J. Special Topics*, vol. 165, no. 1, pp. 73–83, 2008.
[42] R. Zhang and S. Yang, "Robust chaos synchronization of fractional-order chaotic systems with unknown parameters and uncertain perturbations," *Nonlin. Dyn.*, vol. 69, no. 3, pp. 983–992, 2012.
[43] L. Lacasa and J. Gómez-Gardeñes, "Correlation dimension of complex networks," *Phys. Rev. Lett.*, vol. 110, Apr. 2013, Art. no. 168703.
[44] Wikipedia. *Chaos Theory*. Accessed: Apr. 28, 2019. [Online]. Available: https://en.wikipedia.org/wiki/Chaos_theory
[45] P. Grassberger and I. Procaccia, "Characterization of strange attractors," *Phys. Rev. Lett.*, vol. 50, no. 5, p. 346, 1983.
[46] C. M. Danforth, "Chaos in an atmosphere hanging on a wall," in *Mathematics of Planet Earth*. Berlin, Germany: Springer, 2013.
[47] G. Kaddoum, "Wireless chaos-based communication systems: A comprehensive survey," *IEEE Access*, vol. 4, pp. 2621–2648, 2016.
[48] H. Yang, G. Jiang, L. Xia, and X. Tu, "Reference-shifted DCSK modulation scheme for secure communication," in *Proc. Int. Conf. Comput. Netw. Commun. (ICNC)*, 2017, pp. 1073–1076.

Zhongyun Hua (S'14–M'16) received the B.S. degree from Chongqing University, Chongqing, China, in 2011, and the M.S. and Ph.D. degrees from the University of Macau, Macau, China, in 2013 and 2016, respectively, all in software engineering.

He is currently an Associate Professor with the School of Computer Science and Technology, Harbin Institute of Technology Shenzhen, Shenzhen, China. His current research interests include chaotic system, chaos-based applications, and multimedia security.

Yicong Zhou (M'07–SM'14) received the B.S. degree from Hunan University, Changsha, China, in 1992, and the M.S. and Ph.D. degrees from Tufts University, Medford, MA, USA, in 2008 and 2010, respectively, all in electrical engineering.

He is an Associate Professor and the Director of the Vision and Image Processing Laboratory, Department of Computer and Information Science, University of Macau, Macau, China. His current research interests include chaotic systems, multimedia security, computer vision, and machine learning.

Dr. Zhou was a recipient of the Third Price of Macau Natural Science Award in 2014. He serves as an Associate Editor for the IEEE TRANSACTIONS ON CIRCUITS AND SYSTEMS FOR VIDEO TECHNOLOGY, the IEEE TRANSACTIONS ON GEOSCIENCE AND REMOTE SENSING, and several other journals. He is the Co-Chair of the Technical Committee on Cognitive Computing in the IEEE Systems, Man, and Cybernetics Society. He is a Senior Member of the International Society for Optical Engineering (SPIE).